Mon. Not. R. Astron. Soc. **351,** 1204–1214 (2004) doi:10.1111/j.1365-2966.2004.07861.x

# Red giant branch in near-infrared colour–magnitude diagrams – I. Calibration of photometric indices

E. Valenti,[1,2]★ F. R. Ferraro[1] and L. Origlia[2]

[1]*Dipartimento Astronomia, Università di Bologna, Via Ranzani 1, I-40127 Bologna, Italy*
[2]*INAF-Osservatorio Astronomico di Bologna, Via Ranzani 1, I-40127 Bologna, Italy*

Accepted 2004 March 18. Received 2004 March 15; in original form 2004 January 19

**ABSTRACT**

We present new high-quality near-infrared photometry of 10 Galactic globular clusters spanning a wide metallicity range ($-2.12 \leqslant [\mathrm{Fe/H}] \leqslant -0.49$): five clusters belong to the halo (NGC 288, 362, 6752, M15 and M30) and five (NGC 6342, 6380, 6440, 6441 and 6624) to the bulge. By combining $J$, $H$ and $K$ observations with optical data, we constructed colour–magnitude diagrams in various planes: ($K$, $J$–$K$), ($K$, $V$–$K$), ($H$, $J$–$H$) and ($H$, $V$–$H$). A set of photometric indices (colours, magnitudes and slopes) describing the location and the morphology of the red giant branch (RGB) have been measured. We have combined this new data set with those collected by our group over the last 5 years, and here we present an updated calibration of the various RGB indices in the Two-Micron All-Sky Survey photometric system, in terms of the cluster metallicity.

**Key words:** techniques: photometric – stars: evolution – stars: Population II – infrared: stars.

## 1 INTRODUCTION

The study of stellar evolutionary sequences finds several applications in astrophysics: inferring the age and metallicity of stellar systems, synthesizing integrated spectra of galaxies, calibrating standard candles for distance determinations. There are a small number of physical observables that models can predict and that can be compared with observed quantities. Within this framework, the colour–magnitude diagram (CMD) and the luminosity function (LF) are the most powerful tools to test theoretical models, being related to the stellar effective temperature, luminosity and the duration of a specific evolutionary phase (Renzini & Fusi Pecci 1988). In this context, our group started a long-term project devoted to analysing and testing each individual evolutionary sequence in the CMD of Galactic globular clusters (GGCs; see, for example, Ferraro et al. 1999, 2000, hereafter F99 and F00, respectively). In particular, CMDs and LFs in the near-infrared (near-IR) are useful in order to perform a detailed study of the red giant branch (RGB). In fact, in studying cool stellar populations (i.e. RGB stars), the near-IR spectral domain offers several advantages, being the most sensitive to low temperature. Moreover, the background contamination by main-sequence (MS) stars is much less severe, thus allowing us to properly characterize the RGB even in the innermost core region of stellar clusters affected by crowding. In addition, with respect to the visual range, in the IR range the reddening is much lower and, in some cases, when the extinction is very large, as in the bulge, it represents the only possibility to observe the stellar population along the entire RGB. This has been well known for two decades, and several authors have used IR photometry to derive the main RGB properties (see, for example, F00 and references therein).

By combining near-IR and optical photometry we can also calibrate a few major indices with a wide spectral baseline, such as for example the ($V$–$K$) colour, which turn out to be very sensitive to the stellar temperature. In this framework, F00, Valenti et al. (2004a, hereafter V04) and Sollima et al. (2004, hereafter S04) presented near-IR CMDs of a total sample of 16 GGCs (10 in F00, five in V04 and one in S04) which have been used to calibrate several observables describing the RGB physical and chemical properties, and to detect the major RGB evolutionary features (i.e. the bump and the tip).

In this paper we present an additional sample of 10 clusters belonging to different Galactic populations: five clusters (NGC 288, 362, 6752, M15 and M30) belong to the halo and five (NGC 6342, 6380, 6441, 6440 and 6624) belong to the bulge. By combining the data set presented here and the data by F00, V04 and S04 we have now available a homogeneous near-IR data base of 24 GGCs distributed over a wide metallicity range, $-2.12 \leqslant [\mathrm{Fe/H}] \leqslant -0.49$. In this first paper we present the new data set and the calibration of the various RGB photometric parameters (colours at fixed magnitudes, magnitudes at fixed colours, slope) as a function of the cluster metallicity. This work represents an update of the calibrations presented by F00, based on a significantly larger sample (especially in the high metallicity domain). Moreover, because $H$-band observations were also available we derive new calibrations of the RGB photometric indices in this band as well, in order to have a more complete set of metallicity tracers in the near-IR bands.

★E-mail: elena.valenti2@studio.unibo.it (EV); ferraro@bo.astro.it (FRF); origlia@bo.astro.it (LO)

A forthcoming paper (Valenti, Ferraro & Origlia 2004b) will be devoted to a discussion of the major evolutionary features (bump and tip) and their calibration as a function of the metallicity. A third paper (Ferraro et al., in preparation) will deal with the transformation to the theoretical plane and the definition of a useful relation to empirically calibrate the mixing-length parameter of theoretical models.

The observations and data reduction are presented in Section 2, while in Section 3 we describe the properties of the observed CMDs. Section 4 is devoted to deriving the mean RGB features from the CMDs and to a comparison with the previous works. Finally, our conclusions are summarized in Section 5.

## 2 OBSERVATIONS AND DATA REDUCTION

A set of $J$, $H$ and $K$ images was secured at the European Southern Observatory (ESO), La Silla in 1997 August, using the ESO-MPI 2.2-m telescope equipped with the near-IR camera IRAC-2 (Moorwood et al. 1992) based on a NICMOS-3 256 × 256 array detector. The central 4 × 4 arcmin$^2$ region of 10 GGCs, namely NGC 288, 362, 6752, M15, M30, NGC 6342, 6380, 6440, 6441 and 6624, was mapped by using two different magnifications: 0.28 arcsec pixel$^{-1}$ for the most crowed central field and 0.51 arcsec pixel$^{-1}$ for the four fields centred at ∼1 arcmin north-east, north-west, south-east and south-west of the cluster centre. An additional cluster, 47 Tuc, was also observed, but only in the $H$ band. Table 1 lists the observed clusters and their metallicity in the (Carretta & Gratton (1997, hereafter CG97) scale.

During the four observing nights the average seeing was 1–1.2 arcsec. Each $J$, $H$ and $K$ image was the resulting average of 60 exposures of 1-s detector integration time (DIT) and was sky-subtracted and flat-field corrected. The sky field was located several arcmin away from the cluster centre. More details on the pre-reduction procedure can be found in Ferraro et al. (1994) and Montegriffo et al. (1995). The point spread function (PSF) fitting procedure was performed independently on each $J$, $H$ and $K$ image by using the ALLSTAR routine (Stetson & Harris 1988) of the reduction package DAOPHOTII (Stetson 1987). A catalogue listing the instrumental $J$, $H$ and $K$ magnitudes for all the stars identified in each field has been obtained by cross-correlating the single-band catalogues. All stars measured in at least two bands have been included in the final catalogue. Because the observations were performed under not perfect photometric conditions, we transformed the instrumental magnitudes into the Two-Micron All-Sky Survey (2MASS) photometric system.[1] The large number of stars (typically a few hundred) in the overlapping area between our observation and the 2MASS survey were used to derive the calibration to the 2MASS photometric system; only zero-order polynomial relations, without colour terms, have been used.

**Table 1.** The observed sample.

| Name | $[Fe/H]_{CG97}$ | Optical photometry |
|---|---|---|
| Halo clusters | | |
| M15 | −2.12 | Buonanno, Corsi & Fusi Pecci (1985) |
| M30 | −1.91 | Bergbusch (1996) |
| NGC 6752 | −1.42 | Ferraro et al. (2003) |
| NGC 362 | −1.15 | Bellazzini et al. (2001) |
| NGC 288 | −1.07 | Bellazzini et al. (2001) |
| 47 Tuc | −0.70 | Montegriffo et al. (1995) |
| Bulge clusters | | |
| NGC 6380 | −0.87 | Ortolani et al. (1998) |
| NGC 6342 | −0.71 | Piotto et al. (2002) |
| NGC 6441 | −0.68 | Piotto et al. (2002) |
| NGC 6624 | −0.63 | Piotto et al. (2002) |
| NGC 6440 | −0.49 | Ortolani, Bica & Barbuy (1994) |

Because M15 and M30 were observed also by F00, their photometric catalogues were combined with ours in order to reduce the photometric uncertainties. First, the catalogues of M15 and M30 by F00 were transformed in the 2MASS photometric system by using the empirical transformations found by V04. Then, for each cluster we derived a unique catalogue by averaging the multiple measurements.

An overall uncertainty of ±0.05 mag in the zero-point calibration in all three bands has been estimated. Figs 1 and 2 show the $H$, $J–H$ and $K$, $V–K$ CMDs, respectively, for the observed clusters in the 2MASS system.[2]

## 3 COLOUR–MAGNITUDE DIAGRAMS

More than 16 000 and 9000 stars are plotted in the ($H$, $J–H$) and ($K$, $V–K$) CMDs shown in Figs 1 and 2, respectively. The references for the optical data used in this work are listed in Table 1. The main characteristics of the CMDs are schematically summarized as follows.

(i) The RGB is quite well populated in all the programme clusters, even in the brightest magnitude bin, and allows us a clean definition of the mean ridge line, up to the end of the RGB.

(ii) The observations are deep enough to detect the base of the RGB at $\Delta K \sim \Delta H \sim$ 7–8 mag fainter than the RGB tip, and ∼3–4 mag below the horizontal branch (HB).

(iii) In the combined CMDs the HB stars are clearly separable from the RGB stars. For the halo cluster sample, the HB has an almost vertical structure in all the CMDs, as expected for a metal-poor population. The bulge clusters exhibit a red clumpy HB, which is typical of metal-rich populations. In the case of NGC 6441, from the combined CMD it is possible to clearly see the anomalous HB which exhibits both the typical features of metal-poor and metal-rich populations, a red clump and a populated blue branch (see also Rich et al. 1997).

### 3.1 Comparison with previous photometries

Some of the programme clusters, mainly those belonging to the halo, have been the subject of several photometric and spectroscopic observations in the optical bands. For example, NGC 288 and 362 represent an HB ‘second parameter pair’ (see Bellazzini et al. 2001, and references therein), and NGC 6441 has been observed by several authors for its peculiar HB morphology (see Rich et al. 1997, and references therein). However, only a few papers have presented IR photometry for the clusters in our sample. Frogel, Persson & Cohen (1983a) reported $J$, $H$ and $K$ photometry of giants in NGC 288, 362 and 6752. A direct star-to-star comparison was not possible because the authors did not publish the coordinates of the observed stars; nevertheless their photometries nicely overlap our IR CMDs with a minor offset of ≈(0.03–0.05) mag. The comparison of our $K$, $J–K$ CMD of NGC 288 with the mean ridge line published by

[1] In doing this, we used the Second Incremental Release Point Source Catalogue of 2MASS.

[2] The observed cluster catalogues in the 2MASS photometric system are available in electronic form at the CDS.

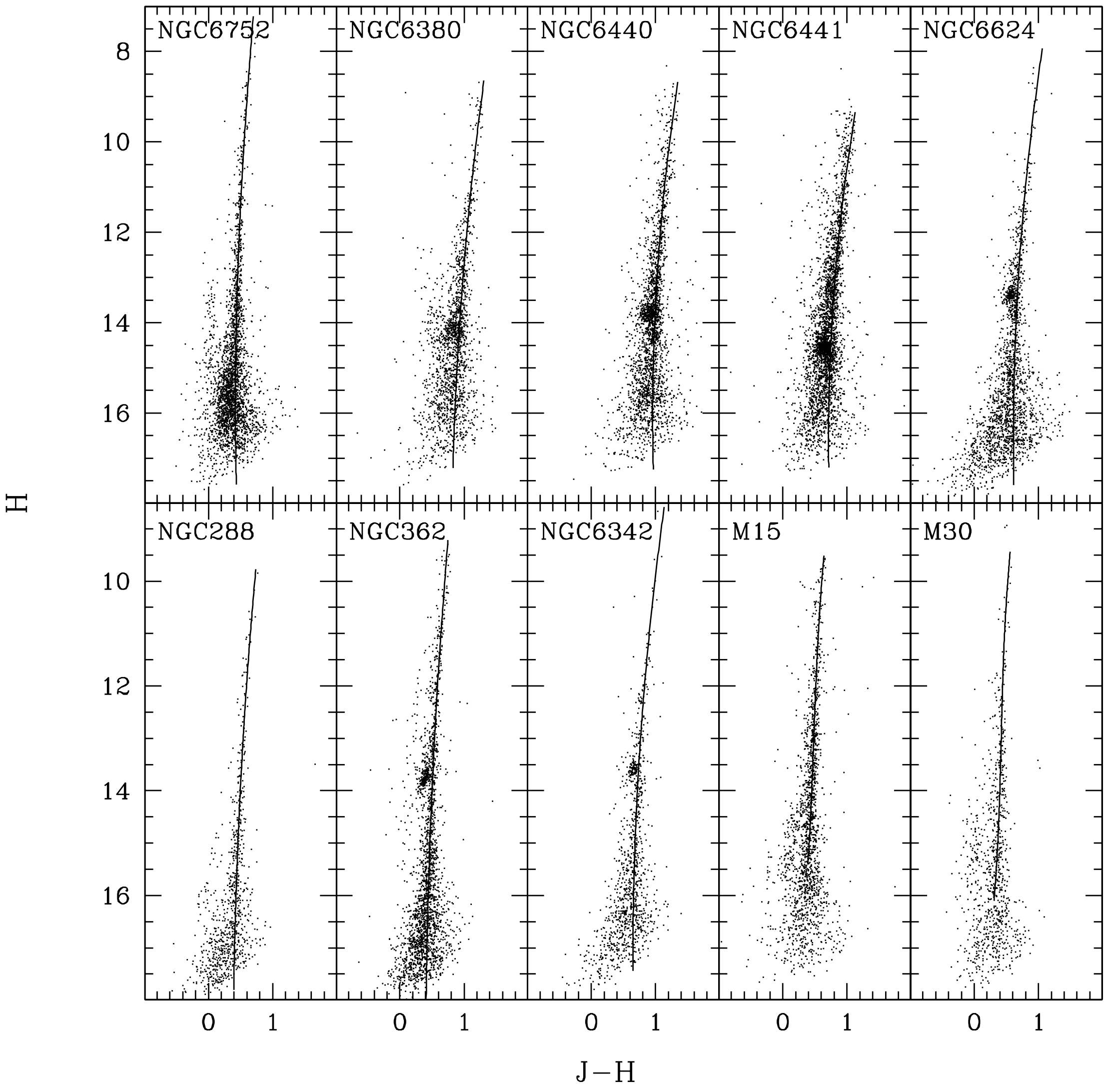


**Figure 1.** *H*, *J–H* CMDs for the 10 GGCs in our data base. The thick line in each panel indicates the RGB fiducial ridge line.

Davidge & Harris (1997) shows a good agreement. For M15 and M30, a comparison with previous photometries can be found in F00.

Conversely, for NGC 6440 and 6624 a star-to-star comparison between our data and the *J*, *H* and *K* photometry published by Kuchinski & Frogel (1995) is possible. They mapped a field of $2.5 \times 2.5$ arcmin$^2$ centred $\sim$1 arcmin north-east from the centre in both clusters, using a 0.35 arcsec pixel$^{-1}$ magnification. An offset of $\approx$0.15 mag was found in all three bands. Also Minniti, Olszewski & Rieke (1995) presented IR photometry of NGC 6440, but no online data are available; however, their data agree with Kuchinski & Frogel (1995). Although the 2MASS photometric system is different from that used by Kuchinski & Frogel (1995), the measured offset seems too large to be due only to the different photometric systems.

IR photometric studies of NGC 6342 and 6380 are not available in the literature.

## 4 MAIN RED GIANT BRANCH FEATURES

The main aim of this series of papers is to present updated calibrations of photometric RGB indices as a function of the metallicity, based on a complete data base collected by our group over the last 10 yr, and presented in F00, V04 and this paper. In this section, the RGB ridge lines and a few major photometric indices, namely colours at fixed magnitudes and magnitudes at fixed colours according to the definitions by F00, are derived from the CMDs shown in Figs 1 and 2. In order to properly combine this data set with those by F00 and V04, we first need to make homogeneous the photometric systems. In particular, we converted the photometry presented in F00 and V04 in the 2MASS system by using the relation found by V04. In the case of $\omega$ Cen, the RGB ridge line was converted into the 2MASS photometric system by using the offset found by S04 ($\Delta J = 0.0$ and $\Delta K = -0.04$). After this transformation, a homogeneous data set of 24 clusters is available. The RGB ridge lines and the photometric indices of the entire sample have been newly determined. Of course, all the known RGB variables lying in the region sampled by our observations (see the cases of 47 Tuc and NGC 6553 in figures 1 and 2 of F00) have been identified and removed from the RGB sample before measuring any parameter.

### 4.1 Red giant branch fiducial ridge lines

Because the procedure to obtain the RGB fiducial ridge lines for the observed clusters has been fully described in F00 and V04, it will not be repeated here. The ridge lines for the 10 clusters presented

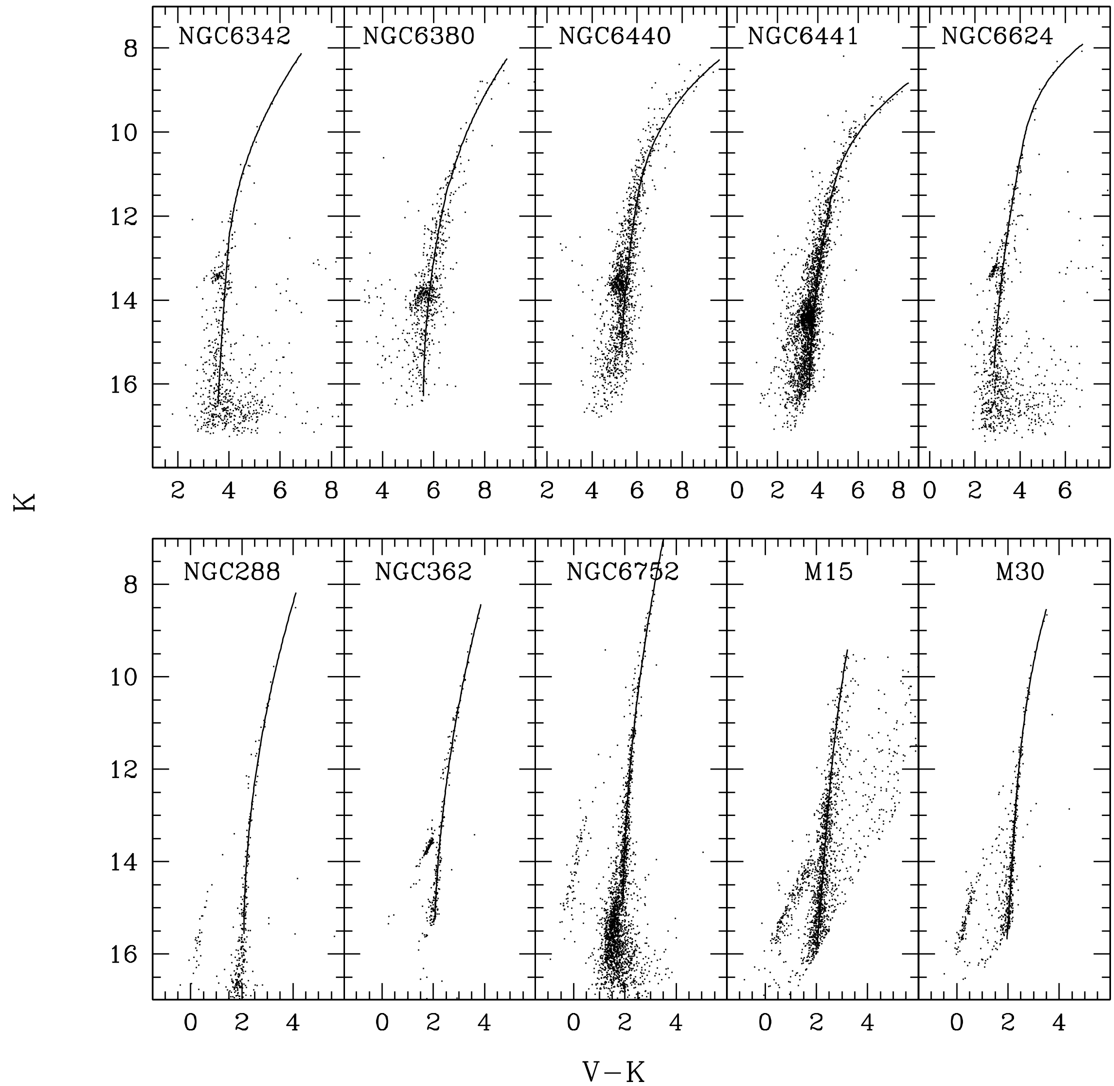


**Figure 2.** *K*, *V–K* CMDs for the 10 GGCs in our data base. The thick line in each panel indicates the RGB fiducial ridge line.

here are overplotted on the (*H*, *J–H*) and (*K*, *V–K*) CMDs shown in Figs 1 and 2, respectively.

### 4.2 Reddening and distance modulus

In order to transform the mean ridge lines into the absolute plane it is necessary to adopt a distance scale and a reddening correction. The definition of the most suitable distance scale for GGCs is still very controversial (see F99 and references therein). In the present study, the distance scale established by F99 was adopted. Nevertheless, in the F99 cluster list (see their table 2) only the halo cluster samples are considered. For the bulge clusters we derived an independent distance modulus from the IR photometry presented here. In doing this, we compared the IR and combined CMDs of the bulge clusters with those of a reference cluster. This method allows us, in principle, to derive simultaneously distance modulus and reddening estimates. In fact, the colour and magnitude shifts needed to overlap the CMDs of two clusters of comparable age and metallicity are a function of the reddening and distance differences, respectively. Because several works on dating bulge GCs have shown that halo and bulge GCs have comparable age (see, for example, Heasley et al. 2000; Ortolani et al. 2001; Feltzing & Johnson 2002; Momany et al. 2003), and because our bulge cluster sample has a metallicity comparable to that of 47 Tuc (within 0.2 dex, see Table 1), we decided to adopt 47 Tuc as a reference cluster. Moreover, the reddening, the metallicity and the distance of 47 Tuc are reasonably known, as it has been one of the most studied GGCs for many decades. As can be seen from Table 2, the reddening determination of the bulge clusters is also quite uncertain (compare the values listed by Harris 1996 with the most recent determination by Schlegel, Finkbeiner & Davis 1998). Of course, a different assumption on the reddening significantly affects the position of the RGB in the absolute plane and the determination of the true distance modulus. For this reason we used the differential analysis described above, in order to derive an independent reddening estimate and to decide the most appropriate reddening for each bulge cluster in our sample. Of course, the position of the RGB in the CMD is a sensitive function of the metallicity and, for this reason, the differential method should be applied to clusters with similar metallicity. From the relations found by F00 we estimate that a difference of ≈0.2 dex in metallicity would produce a difference of ≈0.04 in the (*J–K*) colour and ≈0.1 in (*V–K*).

**Table 2.** Reddening estimates for the programme bulge clusters.

| Cluster | $[Fe/H]_{CG97}$ | $E(B-V)_{Harris96}$ | $E(B-V)_{Schlegel98}$ | $E(B-V)_{derived}$ | $E(B-V)_{adopted}$ |
|---|---|---|---|---|---|
| NGC 6342 | −0.71 | 0.46 | 0.57 | 0.56 | 0.57 |
| NGC 6380 | −0.87 | 1.17 | 1.52 | 1.29 | 1.29 |
| NGC 6441 | −0.68 | 0.44 | 0.63 | 0.52 | 0.52 |
| NGC 6624 | −0.63 | 0.28 | 0.14 | 0.34 | 0.28 |
| NGC 6440 | −0.49 | 1.07 | 1.15 | 1.17 | 1.15 |

As can be seen from Table 1, three bulge clusters in our sample (NGC 6342, 6624 and 6441) have a metallicity (in the CG97 scale) comparable to 47 Tuc (within 0.1 dex). NGC 6380 has a nominal metallicity 0.2 dex lower than 47 Tuc, but the well-defined HB clump and the RGB shape suggest a higher metallicity for this cluster. Previous papers (e.g. Ortolani, Bica & Barbuy 1998) have already suggested for NGC 6380 a metallicity between 47 Tuc and NGC 6553. Finally, NGC 6440 is ≈0.2 dex more metal-rich than the reference cluster. We applied the differential method to the bulge clusters in our sample, and the shifts in colours in different planes, i.e. $\delta(J-H)$, $\delta(J-K)$, $\delta(V-J)$, $\delta(V-H)$ and $\delta(V-K)$, have been computed. Then, by adopting extinction coefficient for the $V$, $J$, $H$ and $K$ bands listed by Savage & Mathis (1979) [$A_V/E(B-V) = 3.1$, $A_J/E(B-V) = 0.87$, $A_H/E(B-V) = 0.54$ and $A_K/E(B-V) = 0.38$] we derived the average value for the reddening. The result of this procedure is shown in Table 2. As can be seen, the value found by our procedure is similar to that found by Schlegel et al. (1998) for NGC 6440 and 6342, while it is more similar to the Harris (1996) value for NGC 6624. For two clusters in our sample, NGC 6380 and 6441, the reddening obtained by our procedure is significantly different (and intermediate) from both values in the literature. For these two clusters we will adopt our reddening value. However, to be conservative, these two clusters are not considered in deriving the relations between the position in colour of the RGB and the cluster metallicity (in different planes). By assuming the reddening listed in column 6 of Table 2 we derived the distance modulus by comparison with 47 Tuc. The HB clump has been chosen as a reference sequence.

The adopted method can be summarized as follows.

(i) The LFs in the IR passbands have been constructed to identify the HB peak, which has been used as the HB level.

(ii) By using the LFs, we measured the differences between the 47 Tuc HB level and those of the bulge clusters; the derived values have been adopted to shift the cluster CMD on the reference one.

(iii) Finally, the differences in magnitudes measured in the various bands have been corrected for reddening (by using the relations quoted above) and the true distance modulus has been obtained.

It is worth noting that, in applying this method, all the available photometric bands were used in order to obtain a more careful estimate. Table 3 lists the adopted distance modulus for all the programme clusters.

Fig. 3 shows the observed RGB fiducial ridge lines in the absolute $M_K$, $(J-K)_0$ and $M_K$, $(V-K)_0$ planes for the entire data base of 24 GGCs (the 10 clusters presented here are plotted as solid lines). As expected, the mean ridge lines of our five intermediate–low-metallicity clusters lie in the bluer region of the diagrams, while in the redder part we find those of high-metallicity clusters of the bulge. A similar behaviour can be seen in Fig. 4, which shows the RGB ridge lines in the absolute $M_H$, $(J-H)_0$ and $M_H$, $(V-H)_0$ planes. In the $M_H$, $(V-H)_0$ plane, the two different groups are more clearly distinguished. The halo cluster RGB lines are bluer and less curved than the RGB lines of the more metal-rich bulge clusters.

**Table 3.** Adopted parameters for the observed GGCs.

| Name | $[Fe/H]_{CG97}$ | [M/H] | $E(B-V)$ | $(m-M)_0$ |
|---|---|---|---|---|
| M15[a] | −2.12 | −1.91 | 0.09 | 15.15 |
| M30[a] | −1.91 | −1.71 | 0.03 | 14.71 |
| NGC 6752[a] | −1.42 | −1.21 | 0.04 | 13.18 |
| NGC 362[a] | −1.15 | −0.99 | 0.05 | 14.68 |
| NGC 288[a] | −1.07 | −0.85 | 0.03 | 14.73 |
| NGC 6380 | −0.87 | −0.68 | 1.29 | 14.81 |
| NGC 6342 | −0.71 | −0.53 | 0.57 | 14.63 |
| NGC 6624 | −0.63 | −0.48 | 0.28 | 14.63 |
| NGC 6441 | −0.68 | −0.52 | 0.52 | 15.65 |
| NGC 6440 | −0.49 | −0.40 | 1.15 | 14.58 |
| 47 Tuc[a] | −0.70 | −0.59 | 0.04 | 13.32 |

[a]For these clusters the estimates listed in table 2 of F99 have been used.

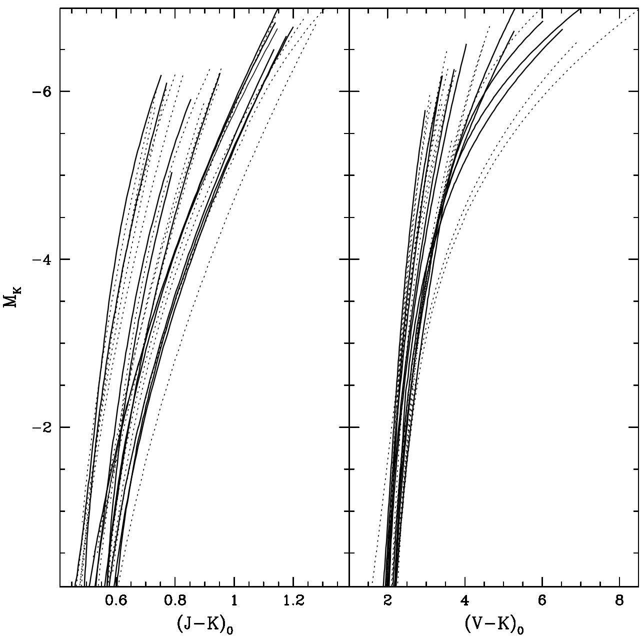


**Figure 3.** RGB fiducial ridge lines for the observed GGCs (solid lines) in $M_K$, $(J-K)_0$ (left panel) and $M_K$, $(V-K)_0$ (right panel). The mean ridge lines for the clusters presented by F00, V04 and S04 (transformed in the 2MASS photometric system) are plotted as dotted lines.

## 4.3 Red giant branch location in colour and in magnitude

As already discussed in detail by F00, to properly characterize the overall behaviour of the RGB as a function of the cluster metallicity, a set of photometric indices is needed (see Section 4). In fact, at fixed colours the corresponding magnitudes mark different RGB regions,

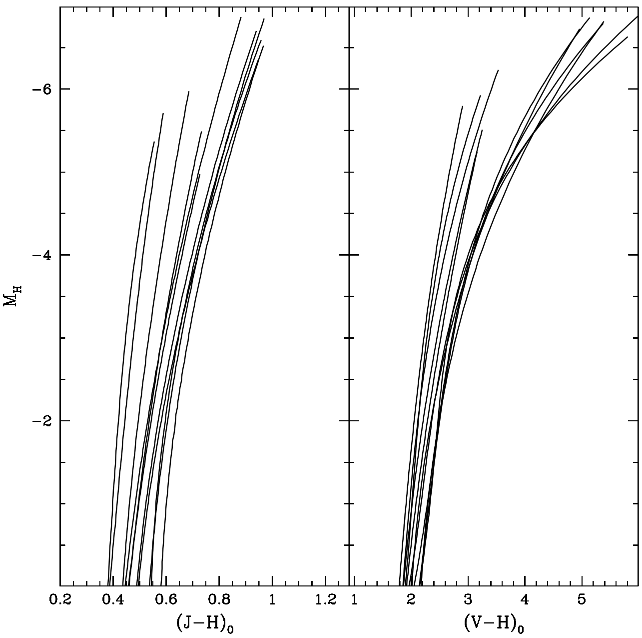


**Figure 4.** RGB fiducial ridge lines for the 10 observed GGCs and for 47 Tuc, in $M_H$, $(J-H)_0$ (left panel) and $M_H$, $(V-H)_0$ (right panel).

depending on the cluster metallicity. Several parameters describing the RGB location in colour and in magnitude have been suggested by many authors (see F00 and references therein). Nevertheless, to obtain a complete description of the RGB photometric properties, in the present study we use the new parameters defined by F00, namely the $(J-K)_0$ and $(V-K)_0$ colours at different absolute magnitudes $M_K = (-3, -4, -5, -5.5)$, and the $K$ absolute magnitude at fixed $(J-K)_0$ and $(V-K)_0$ colours, respectively. The derived $(J-K)_0$ and $(V-K)_0$ RGB colours for the programme clusters are listed in Tables 4 and 5, respectively. In both tables, the measurements by F00 and V04, converted into the 2MASS photometric system, are also reported. The colours at fixed magnitudes for all the clusters in the data base have been calibrated as a function of (i) the metallicity in the CG97 scale, and (ii) the global metallicity ([M/H]) defined and computed in F99, which takes into account the contribution of the $\alpha$-elements in the definition of the global metallicity of the cluster. The metallicity in the CG97 scale for the programme clusters has been computed from the Zinn (1985) scale by using equation (7) of CG97, following the prescriptions by F99. The typical uncertainty on the derived metallicities can be conservatively assumed to be 0.2 dex; however, for clusters having direct CG97 measurements the error is significantly lower, <0.1 dex, (see table 8 of CG97).

The calibration relations of the RGB photometric indices as a function of the cluster metallicity in both the adopted scales are listed in Appendix A.

The cases of NGC 6553 and 6528 (the two clusters which represent the metal-rich extreme of our entire data base) deserve a few additional comments. The metallicity of these two clusters has been, in fact, largely debated in the literature. By simply considering the most recent determinations based on high-resolution spectroscopy, values ranging from $-0.3$ up to about solar (Carretta, Cohen & Gratton 2001; Origlia, Rich & Castro 2002; Meléndez et al. 2003) have been proposed. To be homogeneous with other clusters, for NGC 6553 and 6528 in the following calibrations we will adopt the CG97 values listed in Table 5. Figs 5 and 6 show the $(J-K)_0$ and $(V-K)_0$ colours as a function of both the CG97 and global

**Table 4.** RGB location in colour (columns 4–7), in magnitude (column 8) in the $K$, $J$–$K$ plane and the RGB slope (column 9) for the observed GCs and for the F00, V04 and S04 samples.

| Name | [Fe/H]$_{CG97}$ | [M/H] | $(J-K)_0^{-5.5}$ | $(J-K)_0^{-5}$ | $(J-K)_0^{-4}$ | $(J-K)_0^{-3}$ | $M_K^{(J-K)=0.7}$ | RGB$_{Slope}$ |
|---|---|---|---|---|---|---|---|---|
| M15 | −2.12 | −1.91 | 0.725 ± 0.025 | 0.690 ± 0.023 | 0.629 ± 0.022 | 0.577 ± 0.020 | −5.14 ± 0.27 | −0.044 ± 0.003 |
| M30 | −1.91 | −1.71 | 0.689 ± 0.016 | 0.653 ± 0.014 | 0.597 ± 0.012 | 0.558 ± 0.011 | −5.63 ± 0.19 | −0.044 ± 0.004 |
| NGC 6752 | −1.42 | −1.21 | 0.811 ± 0.018 | 0.766 ± 0.016 | 0.693 ± 0.014 | 0.639 ± 0.012 | −4.10 ± 0.21 | −0.048 ± 0.003 |
| NGC 362 | −1.15 | −0.99 | 0.882 ± 0.017 | 0.837 ± 0.017 | 0.761 ± 0.014 | 0.697 ± 0.013 | −3.06 ± 0.22 | −0.074 ± 0.003 |
| NGC 288 | −1.07 | −0.85 | 0.822 ± 0.015 | 0.786 ± 0.015 | 0.718 ± 0.014 | 0.663 ± 0.013 | −3.69 ± 0.23 | −0.071 ± 0.004 |
| NGC 6380 | −0.87 | −0.68 | 0.954±0.052 | 0.895±0.052 | 0.789±0.051 | 0.697±0.050 | −3.03 ± 0.33 | −0.094 ± 0.003 |
| NGC 6342 | −0.71 | −0.53 | 1.005 ± 0.053 | 0.946 ± 0.052 | 0.840 ± 0.051 | 0.749 ± 0.051 | −2.36 ± 0.39 | −0.102 ± 0.003 |
| NGC 6441 | −0.68 | −0.52 | 0.958±0.053 | 0.898±0.052 | 0.792±0.051 | 0.707±0.050 | −2.91 ± 0.39 | −0.092 ± 0.005 |
| NGC 6624 | −0.63 | −0.48 | 1.023 ± 0.052 | 0.962 ± 0.052 | 0.855 ± 0.051 | 0.764 ± 0.051 | −2.16 ± 0.36 | −0.095 ± 0.003 |
| NGC 6440 | −0.49 | −0.40 | 1.020 ± 0.053 | 0.957 ± 0.052 | 0.847 ± 0.051 | 0.753 ± 0.051 | −2.38 ± 0.40 | −0.093 ± 0.005 |
| M68 | −1.99 | −1.81 | 0.712 ± 0.013 | 0.683 ± 0.013 | 0.629 ± 0.012 | 0.582 ± 0.012 | −5.29 ± 0.22 | −0.048 ± 0.003 |
| M55 | −1.61 | −1.41 | 0.735 ± 0.023 | 0.694 ± 0.023 | 0.629 ± 0.021 | 0.578 ± 0.021 | −5.07 ± 0.30 | −0.049 ± 0.003 |
| M4 | −1.19 | −0.94 | 0.864 ± 0.028 | 0.821 ± 0.027 | 0.741 ± 0.027 | 0.671 ± 0.026 | −3.43 ± 0.40 | −0.079 ± 0.009 |
| M107 | −0.87 | −0.70 | 0.966 ± 0.031 | 0.903 ± 0.031 | 0.790 ± 0.029 | 0.696 ± 0.027 | −3.05 ± 0.33 | −0.075 ± 0.005 |
| 47 Tuc | −0.70 | −0.59 | 1.003 ± 0.018 | 0.934 ± 0.016 | 0.819 ± 0.014 | 0.729 ± 0.012 | −2.61 ± 0.16 | −0.110 ± 0.002 |
| M69 | −0.68 | −0.55 | 0.964 ± 0.031 | 0.906 ± 0.030 | 0.804 ± 0.028 | 0.717 ± 0.027 | −2.79 ± 0.38 | −0.092 ± 0.002 |
| NGC 6553 | −0.44 | −0.36 | 1.036 ± 0.052 | 0.971 ± 0.053 | 0.852 ± 0.052 | 0.753 ± 0.051 | −2.34 ± 0.34 | −0.092 ± 0.002 |
| NGC 6528 | −0.38 | −0.31 | 1.097 ± 0.053 | 1.034 ± 0.052 | 0.919 ± 0.052 | 0.818 ± 0.051 | −1.60 ± 0.38 | −0.114 ± 0.002 |
| M92 | −2.16 | −1.95 | 0.701 ± 0.014 | 0.670 ± 0.013 | 0.611 ± 0.013 | 0.563 ± 0.012 | −5.48 ± 0.21 | −0.046 ± 0.003 |
| M10 | −1.41 | −1.25 | 0.735 ± 0.026 | 0.703 ± 0.026 | 0.644 ± 0.026 | 0.591 ± 0.026 | −4.94 ± 0.43 | −0.048 ± 0.005 |
| M13 | −1.39 | −1.18 | 0.877 ± 0.018 | 0.831 ± 0.017 | 0.746 ± 0.015 | 0.672 ± 0.014 | −3.39 ± 0.20 | −0.065 ± 0.002 |
| M3 | −1.34 | −1.16 | 0.827 ± 0.019 | 0.779 ± 0.016 | 0.705 ± 0.013 | 0.652 ± 0.012 | −3.92 ± 0.21 | −0.071 ± 0.003 |
| M5 | −1.11 | −0.90 | 0.889 ± 0.017 | 0.844 ± 0.016 | 0.764 ± 0.015 | 0.693 ± 0.014 | −3.09 ± 0.21 | −0.082 ± 0.004 |
| $\omega$ Cen | −1.60 | −1.39 | 0.766 ± 0.020 | 0.728 ± 0.020 | 0.660 ± 0.020 | 0.599 ± 0.020 | −4.602 ± 0.19 | −0.050 ± 0.003 |

**Table 5.** RGB $(V–K)_0$ colours at fixed magnitudes $M_K = (-5.5, -5, -4, -3)$ and $K$ absolute magnitude at constant $(V–K)_0$ colour for the observed GCs and for the F00, V04 and S04 samples.

| Name | $[\mathrm{Fe/H}]_{\mathrm{CG97}}$ | [M/H] | $(V-K)_0^{-5.5}$ | $(V-K)_0^{-5}$ | $(V-K)_0^{-4}$ | $(V-K)_0^{-3}$ | $M_K^{(V-K)_0=3}$ |
|---|---|---|---|---|---|---|---|
| M15 | −2.12 | −1.91 | 2.886 ± 0.118 | 2.743 ± 0.116 | 2.505 ± 0.113 | 2.315 ± 0.112 | −5.86 ± 0.38 |
| M30 | −1.91 | −1.71 | 3.106 ± 0.083 | 2.914 ± 0.077 | 2.611 ± 0.067 | 2.392 ± 0.062 | −5.23 ± 0.21 |
| NGC 6752 | −1.42 | −1.21 | 3.157 ± 0.074 | 2.993 ± 0.072 | 2.696 ± 0.068 | 2.441 ± 0.064 | −5.02 ± 0.23 |
| NGC 362 | −1.15 | −0.99 | 3.389 ± 0.083 | 3.189 ± 0.080 | 2.831 ± 0.075 | 2.532 ± 0.068 | −4.49 ± 0.22 |
| NGC 288 | −1.07 | −0.85 | 3.504 ± 0.089 | 3.280 ± 0.085 | 2.889 ± 0.076 | 2.569 ± 0.069 | −4.30 ± 0.20 |
| NGC 6380 | −0.87 | −0.68 | 3.938±0.294 | 3.601±0.288 | 3.051±0.291 | 2.703±0.276 | −3.87 ± 0.46 |
| NGC 6342 | −0.71 | −0.53 | 4.078 ± 0.301 | 3.681 ± 0.295 | 3.049 ± 0.284 | 2.635 ± 0.276 | −3.90 ± 0.33 |
| NGC 6441 | −0.68 | −0.52 | 4.167±0.331 | 3.674±0.302 | 3.132±0.278 | 2.770±0.277 | −3.64 ± 0.40 |
| NGC 6624 | −0.63 | −0.48 | 3.985 ± 0.308 | 3.622 ± 0.288 | 3.204 ± 0.278 | 2.875 ± 0.276 | −3.40 ± 0.42 |
| NGC 6440 | −0.49 | −0.40 | 4.380 ± 0.337 | 3.827 ± 0.311 | 3.113 ± 0.284 | 2.754 ± 0.275 | −3.77 ± 0.38 |
| M68 | −1.99 | −1.81 | 2.949 ± 0.070 | 2.808 ± 0.067 | 2.562 ± 0.064 | 2.360 ± 0.061 | −5.67 ± 0.24 |
| M55 | −1.61 | −1.41 | 3.094 ± 0.124 | 2.910 ± 0.121 | 2.609 ± 0.116 | 2.379 ± 0.113 | −5.25 ± 0.34 |
| M4 | −1.19 | −0.94 | – | 3.464 ± 0.152 | 3.049 ± 0.148 | 2.706 ± 0.144 | −3.87 ± 0.41 |
| M107 | −0.87 | −0.70 | 3.798 ± 0.161 | 3.535 ± 0.155 | 3.105 ± 0.147 | 2.780 ± 0.142 | −3.71 ± 0.45 |
| 47 Tuc | −0.70 | −0.59 | 3.900 ± 0.099 | 3.559 ± 0.081 | 3.098 ± 0.066 | 2.792 ± 0.060 | −3.72 ± 0.20 |
| M69 | −0.68 | −0.55 | 3.830 ± 0.161 | 3.559 ± 0.157 | 3.094 ± 0.150 | 2.723 ± 0.145 | −3.86 ± 0.33 |
| NGC 6553 | −0.44 | −0.36 | 5.023 ± 0.346 | 4.396 ± 0.323 | 3.480 ± 0.294 | 2.904 ± 0.281 | −3.20 ± 0.33 |
| NGC 6528 | −0.38 | −0.31 | 5.255 ± 0.365 | 4.553 ± 0.334 | 3.561 ± 0.298 | 2.968 ± 0.281 | −3.07 ± 0.34 |
| M92 | −2.16 | −1.95 | 2.978 ± 0.078 | 2.808 ± 0.073 | 2.538 ± 0.065 | 2.342 ± 0.060 | −5.56 ± 0.21 |
| M13 | −1.39 | −1.18 | 3.189 ± 0.086 | 2.987 ± 0.079 | 2.661 ± 0.069 | 2.421 ± 0.063 | −5.03 ± 0.21 |
| M3 | −1.34 | −1.16 | 3.355 ± 0.092 | 3.126 ± 0.086 | 2.768 ± 0.071 | 2.514 ± 0.063 | −4.68 ± 0.21 |
| M5 | −1.11 | −0.90 | 3.310 ± 0.092 | 3.079 ± 0.085 | 2.694 ± 0.076 | 2.380 ± 0.070 | −4.81 ± 0.20 |
| $\omega$ Cen | −1.60 | −1.39 | 3.202±0.030 | 2.988±0.030 | 2.648±0.030 | 2.402±0.030 | −5.03±0.20 |

metallicity scales, for the entire sample of 24 clusters. By using the full data set, updated calibrations have been derived and reported in each panel and in Appendix A. As can be seen from Fig. 5, the RGB $(J–K)_0$ colours linearly scale with the metallicity. As expected from previous studies (see Cohen & Sleeper 1995; F00) the fit slope increases progressively toward the RGB tip. The derived slope values are consistent with those found by F00. Conversely, in the $(V–K)_0$ plane, the best-fitting solution deviates from a linear dependence at higher metallicity (see Figs 6a, b, e and f) even if the Carretta et al. (2001) metallicity estimates for the most metal-rich clusters are adopted. As can be seen, the RGB, particularly near the tip, rapidly becomes redder and redder as the metallicity increases as shown by Cohen & Sleeper (1995) and successively confirmed by F00.

For NGC 6624, Cohen & Sleeper (1995) derived the $(J–K)_0$ and $(V–K)_0$ colours at fixed absolute magnitude $M_K = -4$ and $-5$. Their estimates in the $K$, $(J–K)$ plane (see their table 10) are systematically redder, by ∼0.15 with respect to our determinations. This is due to different reddening and distance assumptions; when we apply their reddening and distance modulus values to our photometry, the difference in the derived $(J–K)_0$ colours is reduced to only ∼0.03 mag. In the $K$, $(V–K)$ plane, a ∼0.1-mag difference remains even when the same reddening and distance modulus are adopted. Conversely, a good agreement in the derived $(V–K)_0^{\mathrm{M_K}} = -5$ colour was found with the value published by Kuchinski & Frogel (1995).

By using $(J–H)_0$ and $(V–H)_0$ colours at different absolute magnitudes $M_H = (-3, -4, -5, -5.5)$, new calibrations have been proposed in the $H$ band. The derived values for the programme clusters are listed in Tables 6 and 7, while Figs 7 and 8 show the behaviour of the $(J–H)_0$ and $(V–H)_0$ colours, respectively, as a function of the cluster metallicity in both the adopted metallicity scales. The best fits to the data are shown in each panel and listed in Appendix A. As expected, the colours become redder with increasing cluster metallicity in a linear way and independently from the height cut in the $H$, $(J–H)$ plane, while at brighter magnitudes the $(V–H)_0$ colour shows a quadratic metallicity dependence.

Following Frogel, Cohen & Persson (1983b) and F00 we also measured the $K$ absolute magnitude at fixed $(V–K)_0 = 3$ and $(J–K)_0 = 0.7$ colours. In Fig. 9 we show the dependence of these parameters on metallicity in both adopted scales, for the entire sample. The best-fitting relations are also reported in each panel. Tables 4 and 5 list the derived $M_K$ magnitudes at constant $(J–K)_0$ and $(V–K)_0$ colours, respectively. While the error associated with the determination of the colours at fixed absolute magnitudes are mainly driven by the uncertainty on the distance modulus, the accuracy on the derived absolute magnitude at fixed colours depends on both distance and reddening uncertainties with almost the same weight. In fact, given the intrinsic steepness of the RGB, especially in the metal-poor range, an error of a few hundredths of magnitude in the reddening correction easily implies 0.15–0.20 mag uncertainty in the derived $M_K$ absolute magnitudes, depending on the height along the RGB (see Fig. 3). By using the same strategy we also derive the $M_H$ absolute magnitude at fixed $(J–H)_0 = 0.7$ and $(V–H)_0 = 3$ colours, listed in Tables 6 and 7 and plotted in Fig. 10 as a function of the metallicity in both adopted scales. The best-fitting relations with the corresponding standard fdeviation are reported in each panel and listed in Appendix A.

### 4.4 Red giant branch slope

A useful parameter to provide a photometric estimate of the cluster metallicity is the so-called RGB slope. This parameter turns out to

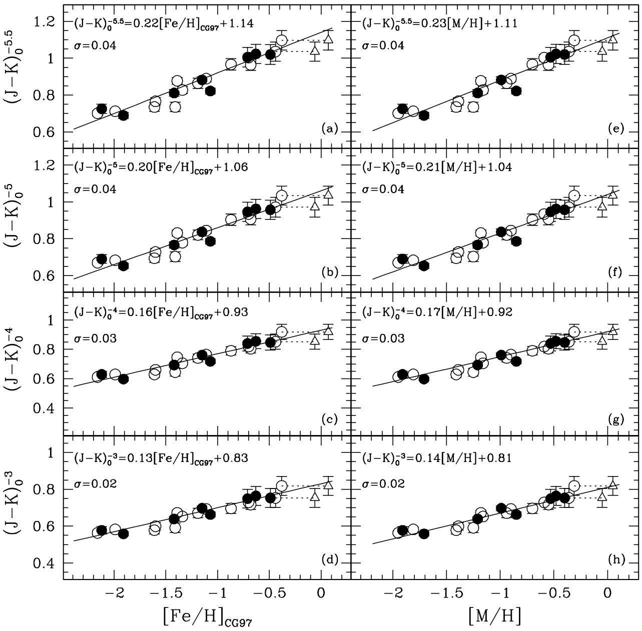


**Figure 5.** RGB mean $(J–K)_0$ colour at fixed $M_K = (-5.5, -5, -4, -3)$ magnitudes as a function of the CG97 metallicity scale (left panels) and of the global metallicity (right panels). Filled circles show the 10 clusters observed here, and empty circles are the F00, V04 and S04 samples. The empty triangles refer to NGC 6553 and 6528 adopting the Carretta et al. (2001) metallicity estimates. The solid lines are best-fitting relations.

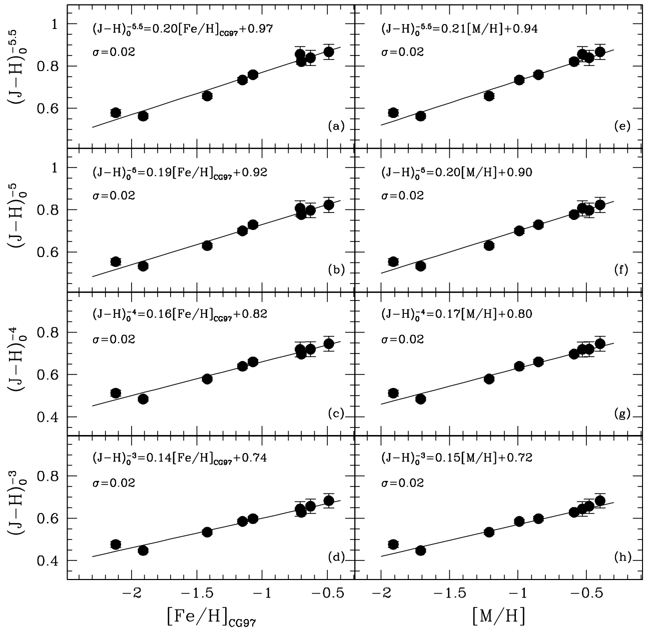


**Figure 7.** RGB mean $(J–H)_0$ colour at fixed ($M_H = -5.5, -5, -4$ and $-3$) magnitudes as a function of the CG97 metallicity scale (left panels) and of the global metallicity (right panels) for the observed clusters. The solid lines are best-fitting relations.

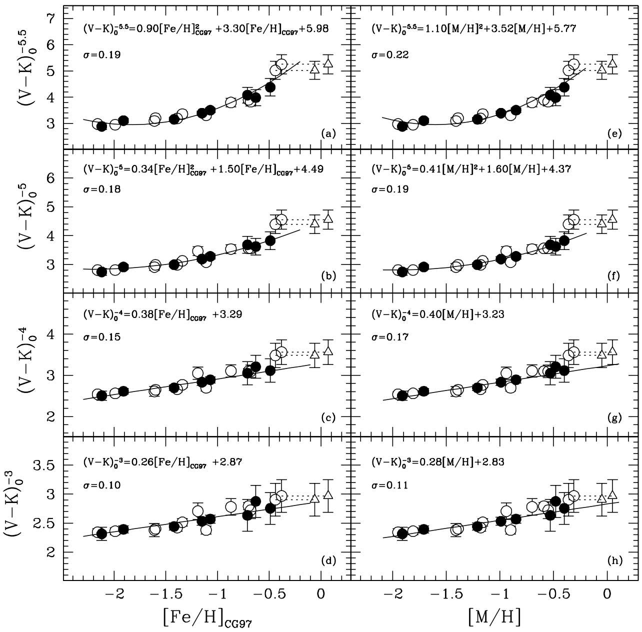


**Figure 6.** The same as Fig. 5, but for $(V–K)_0$ colours.

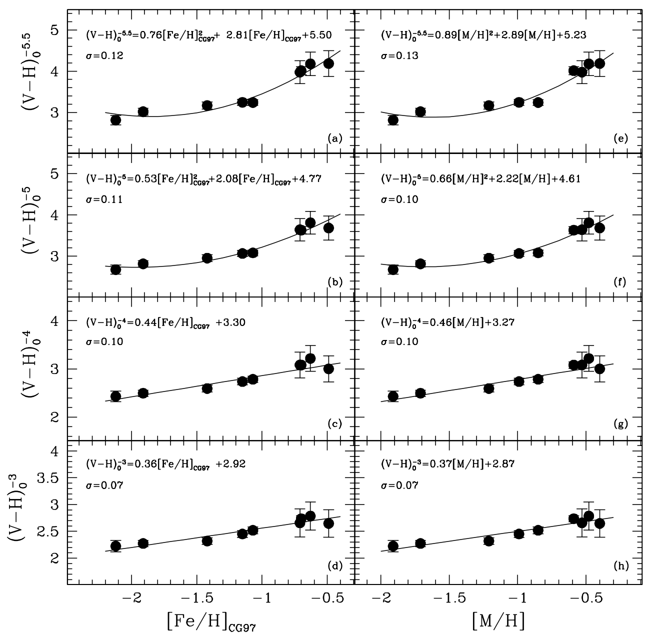


**Figure 8.** The same as Fig. 7, but for $(V–H)_0$ colours.

be extremely powerful because it is independent from reddening and distance. Nevertheless, a careful estimate of the RGB slope is a complicated task, even in the $K$, $(J–K)$ plane, where the RGB is steeper than in any other plane. As shown by Kuchinski et al. (1995) and Kuchinski & Frogel (1995), a reasonable description of the overall RGB morphology can be obtained by linearly fitting the RGB in the range between 0.6 and 5.1 mag brighter than the zero-age horizontal branch (ZAHB). However, in the case of low–intermediate-metallicity clusters the accurate measurement of the location of the ZAHB in the IR CMD is an almost impossible task, because the HB is not horizontal at all. In order to apply a homogeneous procedure to the entire cluster sample, we fit the RGB in a magnitude range between 0.5 and 5 mag fainter than the brightest star of each cluster after a previous decontamination by the asymptotic giant branch (AGB) and field stars. In particular, in the case of the bulge clusters, the level of field contamination was estimated from the comparison with a field CMD obtained from the 2MASS

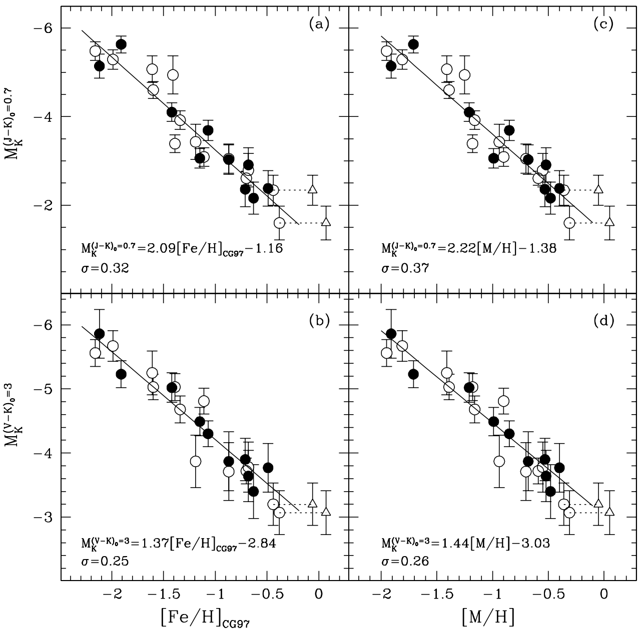


**Figure 9.** Upper panels: $M_K$ at fixed $(J–K)_0 = 0.7$ as a function of the metallicity in the CG97 scale (a) and in the global scale (c). Lower panels: $M_K$ at constant $(V–K)_0 = 3$ as a function of the CG97 metallicity (b) and global metallicity (d). The filled circles refer to the present sample, the empty circles denote the F00, V04 and S04 data and the empty triangles represent NGC 6553 and 6528 adopting the Carretta et al. (2001) metallicity estimates. The solid lines are best-fitting relations.

catalogue for an equivalent area ($4 \times 4$ arcmin$^2$) located at 10 arcmin from the cluster centre. On the basis of this comparison, a typical bulge contamination of 20 per cent was found in the RGB region. Then the estimated number of field stars has been randomly removed from the cluster RGB sample, before determining the RGB slope. The derived RGB slope values for the entire sample are listed in Table 4. Fig. 11 shows the linear correlation of the RGB slope with the metallicity (in both adopted scales); the inferred relations, with the corresponding standard deviations, are also reported in each panel. As expected, the RGB slope becomes progressively steeper with decreasing metallicity,confirming the results found by Kuchinski et al. (1995), Kuchinski & Frogel (1995) and F00. The considerable disagreement between our results and the inferred relations found by Ivanov & Borissova (2002) (dashed lines in Fig. 11), in particular in the high-metallicity range, are mainly due to two different reasons, as follows. (i) Their sample of 22 GCs includes only three clusters more metal-rich than $[\mathrm{Fe/H}]_{\mathrm{CG97}} = -1$ and none more metallic than 47 Tuc, while our best-fitting relations are based on a global sample of 24 clusters, among them seven more metal-rich than 47 Tuc. (ii) There is a discrepancy in the estimate of the 47 Tuc RGB slope: $-0.110 \pm 0.002$ (F00) and $-0.125 \pm 0.002$ (Ivanov & Borissova 2002). Indeed, Ivanov & Borissova (2002) computed a weighed average relation that turned out to be significantly influenced by the value of 47 Tuc, which is the cluster with the most accurate determination.

## 5 SUMMARY AND CONCLUSIONS

We have presented a new set of high-quality IR CMDs for a sample of 10 GGCs spanning a wide metallicity range. This data base has been combined with the data set collected by our group over the last 10 yr (see F00, V04 and S04) and it has been used to measure a few major observables describing the main photometric properties of the RGB: (i) the location in colour and in magnitude, and (ii) its slope.

The behaviour of these quantities as a function of the cluster metallicity has been studied in both $[\mathrm{Fe/H}]_{\mathrm{CG97}}$ and [M/H] metallicity scales. Because our data base also includes observations in the $H$-band, it has been used to derive for the first time the calibrations in the $H$, $J–H$ and $H$, $V–H$ planes as well. All the relations are reported in the corresponding panels of Figs 5–11 and in Appendix A, for more clarity.


## ACKNOWLEDGMENTS

This work is based on data taken at the ESO-MPI 2.2-m telescope equipped with the near-IR camera IRAC2-ESO, La Silla (Chile), within the observing programme 59.E-0340. Part of the data analysis has been performed with the software developed by P. Montegriffo at the Osservatorio Astronomico di Bologna (INAF). This publication makes use of data products from the 2MASS, which is a joint project of the University of Massachusetts and Infrared Processing and Analysis Centre/California Institute of Technology, founded by the National Aeronautics and Space Administration and the National Science Foundation. Financial support by the Agenzia Spaziale Italiana (ASI) and the Ministero dell'Istruzione, Universitá e Ricerca (MIUR) is kindly acknowledged.


**Table 6.** RGB $(J–H)_0$ colours at fixed magnitudes $M_H = (-5.5, -5, -4, -3)$ and $H$ absolute magnitude at constant $(J–H)_0$ for the observed GCs.

| Name | $[\mathrm{Fe/H}]_{\mathrm{CG97}}$ | [M/H] | $(J–H)_0^{-5.5}$ | $(J–H)_0^{-5}$ | $(J–H)_0^{-4}$ | $(J–H)_0^{-3}$ | $(M_H^{(J–H)_0=0.7}$ |
|---|---|---|---|---|---|---|---|
| M15 | −2.12 | −1.91 | 0.579 ± 0.02 | 0.554 ± 0.02 | 0.512 ± 0.02 | 0.476 ± 0.01 | −7.81 ± 0.29 |
| M30 | −1.91 | −1.71 | 0.563 ± 0.01 | 0.533 ± 0.01 | 0.484 ± 0.01 | 0.447 ± 0.01 | −7.63 ± 0.18 |
| NGC 6752 | −1.42 | −1.21 | 0.658 ± 0.01 | 0.630 ± 0.01 | 0.579 ± 0.01 | 0.534 ± 0.01 | −6.28 ± 0.20 |
| NGC 362 | −1.15 | −0.99 | 0.734 ± 0.01 | 0.700 ± 0.01 | 0.639 ± 0.01 | 0.585 ± 0.01 | −5.00 ± 0.19 |
| NGC 288 | −1.07 | −0.85 | 0.759 ± 0.01 | 0.729 ± 0.01 | 0.660 ± 0.01 | 0.598 ± 0.01 | −4.60 ± 0.18 |
| NGC 6380 | −0.87 | −0.68 | 0.762±0.04 | 0.722±0.04 | 0.649±0.04 | 0.585±0.03 | −4.70 ± 0.26 |
| 47 Tuc | −0.70 | −0.59 | 0.821 ± 0.02 | 0.777 ± 0.01 | 0.697 ± 0.01 | 0.628 ± 0.01 | −4.04 ± 0.13 |
| NGC 6342 | −0.71 | −0.53 | 0.856 ± 0.04 | 0.807 ± 0.04 | 0.719 ± 0.04 | 0.644 ± 0.04 | −3.77 ± 0.25 |
| NGC 6441 | −0.68 | −0.52 | 0.841±0.04 | 0.794±0.04 | 0.713±0.04 | 0.646±0.03 | −3.84 ± 0.28 |
| NGC 6624 | −0.63 | −0.48 | 0.839 ± 0.04 | 0.797 ± 0.04 | 0.730 ± 0.04 | 0.657 ± 0.03 | −3.71 ± 0.28 |
| NGC 6440 | −0.49 | −0.40 | 0.867 ± 0.04 | 0.823 ± 0.04 | 0.746 ± 0.04 | 0.683 ± 0.03 | −3.29 ± 0.32 |

**Table 7.** RGB $(V-H)_0$ colours at fixed magnitudes $M_H = (-5.5, -5, -4, -3)$ and $H$ absolute magnitude at constant $(V-H)_0$ colour for the observed GCs.

| Name | $[\mathrm{Fe/H}]_{\mathrm{CG97}}$ | [M/H] | $(V-H)_0^{-5.5}$ | $(V-H)_0^{-5}$ | $(V-H)_0^{-4}$ | $(V-H)_0^{-3}$ | $(M_H^{(V-H)_0=3}$ |
|---|---|---|---|---|---|---|---|
| M15 | −2.12 | −1.91 | 2.815 ± 0.11 | 2.674 ± 0.11 | 2.430 ± 0.11 | 2.224 ± 0.11 | −6.10 ± 0.35 |
| M30 | −1.91 | −1.71 | 3.019 ± 0.09 | 2.814 ± 0.08 | 2.495 ± 0.07 | 2.274 ± 0.06 | −5.46 ± 0.19 |
| NGC 6752 | −1.42 | −1.21 | 3.169 ± 0.09 | 2.952 ± 0.08 | 2.592 ± 0.07 | 2.319 ± 0.06 | −5.11 ± 0.19 |
| NGC 362 | −1.15 | −0.99 | 3.246 ± 0.08 | 3.065 ± 0.07 | 2.737 ± 0.07 | 2.451 ± 0.07 | −4.81 ± 0.21 |
| NGC 288 | −1.07 | −0.85 | 3.242 ± 0.07 | 3.080 ± 0.07 | 2.785 ± 0.07 | 2.520 ± 0.06 | −4.74 ± 0.23 |
| NGC 6380 | −0.87 | −0.68 | 3.880±0.28 | 3.547±0.27 | 3.047±0.27 | 2.717±0.26 | −3.87 ± 0.38 |
| 47 Tuc | −0.70 | −0.59 | 4.012 ± 0.10 | 3.630 ± 0.09 | 3.080 ± 0.07 | 2.736 ± 0.06 | −3.81 ± 0.17 |
| NGC 6342 | −0.71 | −0.53 | 3.975 ± 0.28 | 3.641 ± 0.27 | 3.082 ± 0.27 | 2.659 ± 0.26 | −3.82 ± 0.12 |
| NGC 6441 | −0.68 | −0.52 | 4.175±0.31 | 3.720±0.27 | 3.043±0.27 | 2.624±0.26 | −3.92 ± 0.30 |
| NGC 6624 | −0.63 | −0.48 | 4.177 ± 0.28 | 3.810 ± 0.28 | 3.216 ± 0.27 | 2.785 ± 0.26 | −3.54 ± 0.23 |
| NGC 6440 | −0.49 | −0.40 | 4.186 ± 0.31 | 3.683 ± 0.29 | 3.001 ± 0.27 | 2.647 ± 0.26 | −4.00 ± 0.30 |

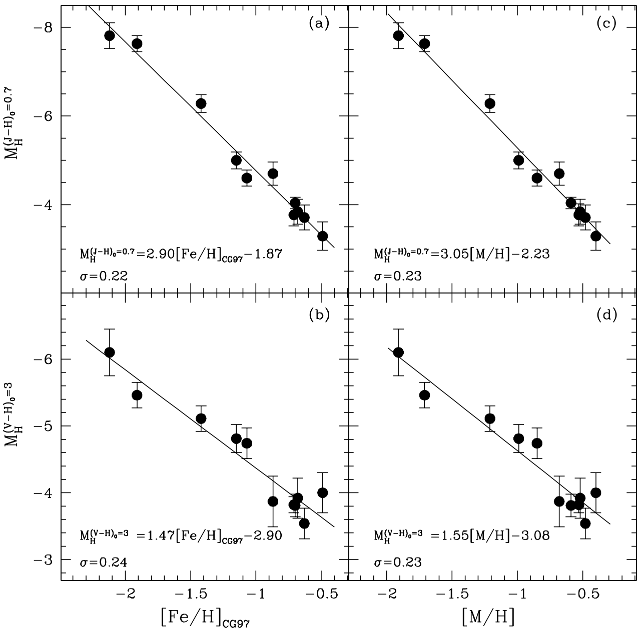


**Figure 10.** The same as Fig. 9, but for $M_H$ magnitudes.

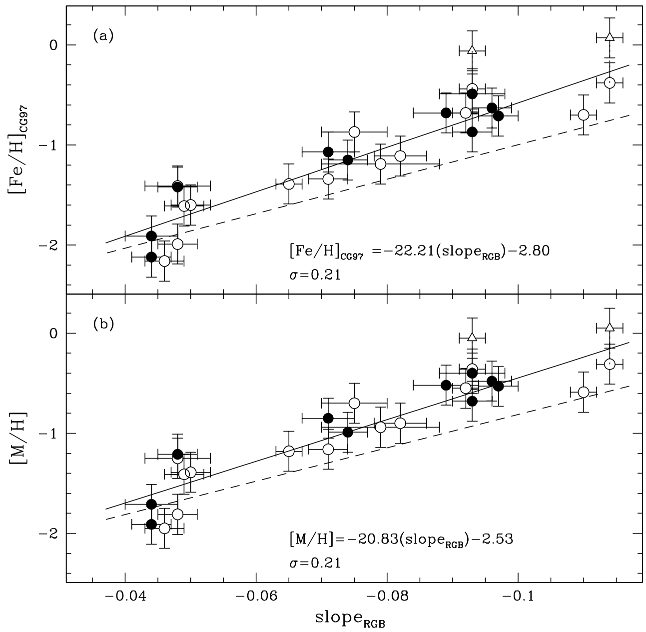


**Figure 11.** Metallicity scale: $[\mathrm{Fe/H}]_{\mathrm{CG97}}$ (a) and [M/H] (b) as a function of the derived RGB slope for the selected 10 GCs (filled circles) and for the F00, V04 and S04 programme clusters (empty circles). The solid lines are our best-fitting relations, while the dashed lines are the relations found by Ivanov & Borissova (2002).

## REFERENCES


Bellazzini M., Fusi Pecci F., Ferraro F. R., Galleti S., Catelan, M., Landsman W. B., 2001, AJ, 122, 2569
Bergbusch P. A., 1996, AJ, 112, 1061
Buonanno R., Corsi C. E., Fusi Pecci F., 1985, A&A, 145, 97
Carretta E., Gratton R. G., 1997, A&AS, 121, 95 (CG97)
Carretta E., Cohen J. G., Gratton R. G., 2001, AJ, 122, 1469
Cohen J. G., Sleeper C., 1995, AJ, 109, 242
Davidge T. J., Harris W. E., 1997, AJ, 475, 584
Feltzing S., Johnson R. A., 2002, A&A, 385, 67
Ferraro F. R., Fusi Pecci F., Guarnieri M. D., Moneti A., Origlia L., Testa V., 1994, MNRAS, 266, 829
Ferraro F. R., Messineo Fusi, Pecci F., De Palo M. A., Straniero O., Chieffi A., Limongi M., 1999, AJ, 118, 1738 (F99)
Ferraro F. R., Montegriffo P., Origlia L., Fusi Pecci F., 2000, AJ, 119, 1282 (F00)
Ferraro F. R., Possenti A., Sabbi E., Lagani P., Rood R. T., D'Amico N., Origlia L., 2003, ApJ, 595, 179
Frogel J. A., Persson S. E., Cohen J. G., 1983a, ApJS, 53, 713
Frogel J. A., Cohen J. G., Persson S. E., 1983b, ApJ, 275, 773
Harris W. E., 1996, AJ, 112, 1487
Heasley J. N., Janes K. A., Zinn R., Demarque P., Da Costa G. S., Christian C. A., 2000, AJ, 120, 879
Ivanov V. D., Borissova J., 2002, A&A, 390, 937
Kuchinski L. E., Frogel J. A., 1995, AJ, 110, 284
Kuchinski L. E., Frogel J. A., Terndrup D. M., Persson S. E., 1995, AJ, 109, 1131
Meléndez J., Barbuy B., Bica E., Zoccali M., Ortolani S., Renzini A., Hill V., 2003, A&A, 411, 417
Minniti D., Olszewski W. E., Rieke M., 1995, AJ, 110, 1686
Momany Y. et al., 2003, A&A, 402, 607
Montegriffo P., Ferraro F. R., Fusi Pecci F., Origlia L., 1995, MNRAS, 276, 739
Moorwood et al., 1992, The Messenger, 69, 61
Origlia L., Rich R. M., Castro S., 2002, AJ, 123, 1559
Ortolani S., Bica E., Barbuy B., 1994, A&AS, 108, 653
Ortolani S., Bica E., Barbuy B., 1998, A&AS, 127, 471
Ortolani S., Barbuy B., Bica E., Renzini A., Zoccali M., Rich R. M., Cassisi S., 2001, A&A, 376, 878
Piotto G. et al., 2002, A&A, 391, 945

Renzini A., Fusi Pecci F., 1988, ARA&A, 26, 199
Rich R. M. et al., 1997, ApJ, 484, 25
Savage B. D., Mathis J. S., 1979, ARA&A, 17, 73
Schlegel D. J., Finkbeiner D. P., Davis M., 1998, ApJ, 500, 525
Sollima A., Ferraro F. R., Origlia L., Pancino E., Bellazzini M., 2004, A&A, in press (astro-ph/0402100)
Stetson P. B., 1987, PASP, 99, 191
Stetson P. B., Harris W. E., 1988, AJ, 96, 909
Valenti E., Ferraro F. R., Perina S., Origlia L., 2004a, A&A, in press (astro-ph/0401153)
Valenti E., Ferraro F. R., Origlia L., 2004b, MNRAS, in press (astro-ph/0404403)
Zinn R., 1985, ApJ, 293, 424

## APPENDIX A: CALIBRATION RELATIONS

In this appendix we report all the relations linking the photometric indices defined in the paper as a function of the cluster metallicity in both the CG97 scale and the global scale.

$(J–K)_0$ colours at fixed $M_K = (-5.5, -5, -4, -3)$ magnitudes:

$$(J-K)_0^{M_K=-5.5} = 0.22[\mathrm{Fe/H}]_{\mathrm{CG97}} + 1.14 \tag{A1}$$

$$(J-K)_0^{M_K=-5} = 0.20[\mathrm{Fe/H}]_{\mathrm{CG97}} + 1.06 \tag{A2}$$

$$(J-K)_0^{M_K=-4} = 0.16[\mathrm{Fe/H}]_{\mathrm{CG97}} + 0.93 \tag{A3}$$

$$(J-K)_0^{M_K=-3} = 0.13[\mathrm{Fe/H}]_{\mathrm{CG97}} + 0.83 \tag{A4}$$

$$(J-K)_0^{M_K=-5.5} = 0.23[\mathrm{M/H}] + 1.11 \tag{A5}$$

$$(J-K)_0^{M_K=-5} = 0.21[\mathrm{M/H}] + 1.04 \tag{A6}$$

$$(J-K)_0^{M_K=-4} = 0.17[\mathrm{M/H}] + 0.92 \tag{A7}$$

$$(J-K)_0^{M_K=-3} = 0.14[\mathrm{M/H}] + 0.81 \tag{A8}$$

$(V - K)_0$ colours at fixed $M_K = (-5.5, -5, -4, -3)$ magnitudes:

$$(V-K)_0^{M_K=-5.5} = 0.90[\mathrm{Fe/H}]^2_{\mathrm{CG97}} + 3.30[\mathrm{Fe/H}]_{\mathrm{CG97}} + 5.98 \tag{A9}$$

$$(V-K)_0^{M_K=-5} = 0.34[\mathrm{Fe/H}]^2_{\mathrm{CG97}} + 1.50[\mathrm{Fe/H}]_{\mathrm{CG97}} + 4.49 \tag{A10}$$

$$(V-K)_0^{M_K=-4} = 0.38[\mathrm{Fe/H}]_{\mathrm{CG97}} + 3.29 \tag{A11}$$

$$(V-K)_0^{M_K=-3} = 0.26[\mathrm{Fe/H}]_{\mathrm{CG97}} + 2.87 \tag{A12}$$

$$(V-K)_0^{M_K=-5.5} = 1.10[\mathrm{M/H}]^2 + 3.52[\mathrm{M/H}] + 5.77 \tag{A13}$$

$$(V-K)_0^{M_K=-5} = 0.41[\mathrm{M/H}]^2 + 1.60[\mathrm{M/H}] + 4.37 \tag{A14}$$

$$(V-K)_0^{M_K=-4} = 0.40[\mathrm{M/H}] + 3.23 \tag{A15}$$

$$(V-K)_0^{M_K=-3} = 0.28[\mathrm{M/H}] + 2.83 \tag{A16}$$

$(J -H)_0$ colours at fixed ($M_H = -5.5, -5, -4$ and $-3$) magnitudes:

$$(J-H)_0^{M_H=-5.5} = 0.20[\mathrm{Fe/H}]_{\mathrm{CG97}} + 0.97 \tag{A17}$$

$$(J-H)_0^{M_H=-5} = 0.19[\mathrm{Fe/H}]_{\mathrm{CG97}} + 0.92 \tag{A18}$$

$$(J-H)_0^{M_H=-4} = 0.16[\mathrm{Fe/H}]_{\mathrm{CG97}} + 0.82 \tag{A19}$$

$$(J-H)_0^{M_H=-3} = 0.14[\mathrm{Fe/H}]_{\mathrm{CG97}} + 0.74 \tag{A20}$$

$$(J-H)_0^{M_H=-5.5} = 0.21[\mathrm{M/H}] + 0.94 \tag{A21}$$

$$(J-H)_0^{M_H=-5} = 0.20[\mathrm{M/H}] + 0.90 \tag{A22}$$

$$(J-H)_0^{M_H=-4} = 0.17[\mathrm{M/H}] + 0.80 \tag{A23}$$

$$(J-H)_0^{M_H=-3} = 0.15[\mathrm{M/H}] + 0.72. \tag{A24}$$

$(V -H)_0$ colours at fixed ($M_H = -5.5, -5, -4$ and $-3$) magnitudes:

$$(V-H)_0^{M_H=-5.5} = 0.76[\mathrm{Fe/H}]^2_{\mathrm{CG97}} + 2.81[\mathrm{Fe/H}]_{\mathrm{CG97}} + 5.50 \tag{A25}$$

$$(V-H)_0^{M_H=-5} = 0.53[\mathrm{Fe/H}]^2_{\mathrm{CG97}} + 2.08[\mathrm{Fe/H}]_{\mathrm{CG97}} + 4.77 \tag{A26}$$

$$(V-H)_0^{M_H=-4} = 0.44[\mathrm{Fe/H}]_{\mathrm{CG97}} + 3.30 \tag{A27}$$

$$(V-H)_0^{M_H=-3} = 0.36[\mathrm{Fe/H}]_{\mathrm{CG97}} + 2.92 \tag{A28}$$

$$(V-H)_0^{M_H=-5.5} = 0.89[\mathrm{M/H}]^2 + 2.89[\mathrm{M/H}] + 5.23 \tag{A29}$$

$$(V-H)_0^{M_H=-5} = 0.66[\mathrm{M/H}]^2 + 2.22[\mathrm{M/H}] + 4.61 \tag{A30}$$

$$(V-H)_0^{M_H=-4} = 0.46[\mathrm{M/H}] + 3.24 \tag{A31}$$

$$(V-H)_0^{M_H=-3} = 0.37[\mathrm{M/H}] + 2.87. \tag{A32}$$

$M_K$ magnitudes at fixed $(J -K)_0 = 0.7$ and $(V–K)_0 = 3$ colours:

$$M_K^{(J-K)_0=0.7} = 2.09[\mathrm{Fe/H}]_{\mathrm{CG97}} - 1.16 \tag{A33}$$

$$M_K^{(V-K)_0=3} = 1.37[\mathrm{Fe/H}]_{\mathrm{CG97}} - 2.84 \tag{A34}$$

$$M_K^{(J-K)_0=0.7} = 2.22[\mathrm{M/H}] - 1.38 \tag{A35}$$

$$M_K^{(V-K)_0=3} = 1.44[\mathrm{M/H}] - 3.03. \tag{A36}$$

$M_H$ magnitudes at fixed $(J–H)_0 = 0.7$ and $(V–H)_0 = 3$ colours:

$$M_H^{(J-H)_0=0.7} = 2.90[\mathrm{Fe/H}]_{\mathrm{CG97}} - 1.87 \tag{A37}$$

$$M_H^{(V-H)_0=3} = 1.47[\mathrm{Fe/H}]_{\mathrm{CG97}} - 2.90 \tag{A38}$$

$$M_H^{(J-H)_0=0.7} = 3.05[\mathrm{M/H}] - 2.23 \tag{A39}$$

$$M_H^{(V-H)_0=3} = 1.55[\mathrm{M/H}] - 3.08. \tag{A40}$$

The RGB slope:

$$[\mathrm{Fe/H}]_{\mathrm{CG97}} = -22.21(\mathrm{slope_{RGB}}) - 2.80 \tag{A41}$$

$$[\mathrm{M/H}] = -20.83(\mathrm{slope_{RGB}}) - 2.53. \tag{A42}$$

This paper has been typeset from a TEX/LATEX file prepared by the author.